

# Cosmological parameter determination from Planck and SDSS data in $\Lambda$ CHDM cosmologies

L.A. Popa<sup>1</sup>

Institute of Space Sciences, Bucharest-Magurele, R-76900, Romania

C. Burigana and N. Mandolesi

Istituto TeSRE, Consiglio Nazionale delle Ricerche, Via Gobetti 101, I-40129 Bologna, Italy

Received \_\_\_\_\_; accepted \_\_\_\_\_

Submitted to ApJ and received, 23 January 2001

---

<sup>1</sup>further address: Istituto TeSRE, Consiglio Nazionale delle Ricerche, Via Gobetti 101,  
I-40129 Bologna, Italy

## ABSTRACT

We study the complementarity between the cosmological information obtainable with the PLANCK surveyour and the large scale structure (LSS) redshift surveys in  $\Lambda$ CHDM cosmologies.

We compute the initial full phase-space neutrino distribution function for  $\Lambda$ CHDM models by using numerical simulations. As initial condition we adopt the HDM density fluctuation power spectrum normalized on the basis of the analysis of the local cluster X-ray temperature function and derive the initial neutrino phase-space distribution at each spatial wave number  $k$  by using the Zel'dovich approximation. These initial neutrino phase-space distributions are implemented in the CMBFAST code for the integration of the coupled linearized Einstein, Boltzmann and fluid equations in  $k$ -space. We find that the relative bias between the CMB temperature fluctuations and the underlying matter density fluctuation power spectrum in COBE/DMR normalization is given by the CDM component normalized accordingly to the abundance of rich clusters at the present time.

We use the Fisher information matrix approximation to constrain a multi-dimensional parametrization of the  $\Lambda$ CHDM model, by jointly considering CMB and large scale structure data according to the PLANCK and the SDSS experimental specifications and by taking into account redshift distortions and nonlinear effects on the matter power spectrum. We found that, although the CMB anisotropy and polarization measurements tend to dominate the constraints on most of the cosmological parameters, the additional small scale LSS data help to break the parameter degeneracies.

This work has been done in the framework of the PLANCK LFI activities.

*Subject headings:* Cosmology: cosmic microwave background – large scale structure – dark matter – Elementary particles

## 1. Introduction

The simplest hypothesis for the origin of the large-scale structure of the present universe is that it is the result of the gravitational instability of small initial density perturbations. In this framework, significant improvements on the study of the formation and evolution of the cosmological large-scale structure have been achieved in the recent years <sup>2</sup>. In the same time, new analysis techniques have been developed in order to extract more sensitively the long-wavelength portion of the power spectrum (see, e.g., Hamilton et al. 1991, Jain, Mo & White 1995, Peacock & Dodds 1996, Ma 1998). The new generation of high precision large scale structure (LSS) redshift surveys such as the Sloan Digital Sky survey<sup>3</sup> (SDSS) and 2dF survey<sup>4</sup> are able to measure the total power spectrum of the matter density fluctuations with high accuracy for comoving wavelengths  $\lambda \gtrsim 20 h^{-1}\text{Mpc}$  ( $h=H_0/100 \text{ Km s}^{-1}\text{Mpc}^{-1}$  is dimensionless Hubble constant), probing the strong clustering regime effects on the power spectrum.

We are also increasingly able to probe the primordial fluctuations through Cosmic Microwave Background (CMB) anisotropy experiments (see, e.g., Tegmark & Zaldarriaga 2000 for a recent compilation). The PLANCK surveyor <sup>5</sup> of ESA will observe the microwave

---

<sup>2</sup><http://star-www.dur.ac.uk/virgo/virgo.html>

<sup>3</sup><http://www.sdss.org>

<sup>4</sup><http://mso.anu.edu.au/colles/2dFGRS>

<sup>5</sup><http://astro.estec.esa.nl/SA-general/Projects/Planck/>

sky anisotropies at frequencies between 30 and 900 GHz with FWHM angular resolutions between  $33'$  and  $5'$  and sensitivities per FWHM side squared pixel at  $\sim 10\mu\text{K}$  level at least for the channels at frequency less than  $\sim 300$  GHz.

The efforts to measure the CMB anisotropy at sub-degree angular scales and galaxy density fluctuations in our local universe can provide independent probes for the structure of the universe on similar comoving scales at different cosmological epochs [the sub-degree angular scales on the last scattering surface of the CMB correspond to comoving scales of  $\sim 50 - 100 h^{-1}$  Mpc in the present local universe: an angle  $\theta$  degrees subtends a comoving distance of  $105\theta(\Omega_0 h)^{-1}$  Mpc]. The comparison between these two type of measurements is an unique way to test the hypothesis of fluctuation growth by gravitational instability; when the time dependence of the galaxy linear bias factor (defined as  $b_I = 1/\sigma_8$ , where  $\sigma_8$  represents the *rms* mass fluctuations in a sphere of radius  $R=8 h^{-1}$  Mpc) is understood the combined data can be also used to constrain the parameters of competing cosmological models (see, e.g., Tegmark 1998, Eisenstein, Hu & Tegmark 1998, Eisenstein, Hu & Tegmark 1999b, Tegmark & Hamilton 2000).

The combined analysis of the CMB data and the local density field fluctuations, as suggested by Juszkiewicz, Górski & Silk (1987), was used to obtain a corresponding CMB map as viewed by a distant observer (Bertschinger, Górsky & Dekel 1990), starting from the density field as derived by the POTENT procedure (Bertschinger et al. 1990, Dekel 1994). Also, by using the likelihood analysis of the MARK III peculiar velocity data, the density power spectrum for a range of parameters within the framework of CDM models normalized to COBE/DMR was translated into a range of angular power spectra of the CMB anisotropy and compared with the CMB observations (Zaroubi et al. 1996). The density field reconstructed via Wiener Filter method was then translated into a map of  $\Delta T/T$  as viewed by a distant observer on his last-scattering surface.

It is difficult in the actual experimental context to explain the observations of the cosmological large scale structure as well as the CMB anisotropy in the frame of the standard Cold Dark Matter (sCDM) model normalized to COBE/DMR data (Smoot et al. 1992, Wright et al. 1994, Górski et al. 1994, Bennett et al. 1996). At small scales, both the amplitude and the shape of the CMB anisotropy power spectrum predicted by this model are inconsistent with the observations of the Large Scale Structure (LSS) of the universe as derived by galaxy surveys (e.g., Scott & White 1994; White et al. 1995; Primack et al. 1995). The small scale power excess with respect to the large scale power can be reduced by the addition of a Hot Dark Matter (HDM) component to the total mass density of the universe in form of massive neutrinos (see, e.g., Primack et al. 1995), also motivated by the recent experimental results of the atmospheric neutrino oscillation experiments (see, e.g., Fukuda et al. 1998, Ambrosio et al. 1998).

On the other hand, evidences have been accumulated that we live in a low matter density universe (see, e.g., Fukugita, Liu & Sugiyama 1999 and the references therein). Indications like the Hubble diagram from Type 1a supernovae (Riess et al. 1998, Perlmutter et al. 1998) and the acoustic peak distribution in the CMB anisotropy power spectrum (Hancock et al. 1998, Efstathiou et al. 1999) point to a universe dominated by vacuum energy, characterized by a cosmological constant  $\Lambda$  that keeps the universe close to be flat. The combined analysis of the CMB anisotropy experiments and Type 1a supernovae observations (Efstathiou et al. 1999) indicates  $\Omega_m = 0.25^{+0.18}_{-0.12}$  and  $\Omega_\Lambda = 0.63^{+0.17}_{-0.23}$  (95% confidence errors) respectively for the total matter and the vacuum energy density normalized to the critical density, inferring a Hubble constant value  $H_0=65 \text{ Km s}^{-1} \text{ Mpc}^{-1}$ .

Current cosmological constraints on the cosmological parameters obtained by using the most recent CMB anisotropy data (Lange et al. 2000, Balbi et al. 2000) combined with Type 1a supernovae data implies a best fit model close to a flat  $\Lambda$ CHDM model having

$\Omega_m \approx 0.33$ ,  $\Omega_\Lambda = 0.67$  and a neutrino density parameter  $\Omega_\nu \approx 0.1$ , when the priors  $H_0 = 65$   $\text{Km s}^{-1} \text{Mpc}^{-1}$  and  $\Omega_b h^2 = 0.02$  are assumed (Tegmark & Zaldarriaga 2000).

The introduction of HDM component in the form of neutrinos with the mass in the eV range suppress the growth of fluctuations on all scales below the neutrino free-streaming scale  $k_{\text{fs}}^2 = 4\pi G \rho a^2 / \langle v \rangle^2$  (Bond & Szalay 1980, Hu & Eisenstein 1998, Ma 1999), where  $G$  is the gravitational constant,  $a$  is the cosmological scale factor ( $a = a_0 = 1$  today),  $\rho$  is the density and  $\langle v \rangle$  is the averaged neutrino speed. The magnitude of the power suppression is given by  $\Delta P/P \approx -8\Omega_\nu/\Omega_m \approx -0.087(m_\nu/\text{eV})(N_\nu/\Omega_m h^2)$ , where  $N_\nu$  is the number of massive neutrino flavours and  $m_\nu$  is the neutrino mass. The time dependence of the free-streaming length implies that neutrinos cluster gravitationally on smaller length scales at latter times (see Ma & Bertschinger 1995, Ma 1996, Ma 1999 for discussions on the time dependence of the free-streaming scale). In the cosmological models involving a HDM contribution to the total energy density, the existence of neutrino free-streaming length scale implies that the growth of the density perturbations depends both on time and spatial wave number  $k$ .

In the linear perturbation theory, the CMB anisotropy and matter transfer function are computed by the integration of coupled and linearized Einstein, Boltzmann and fluid equations (Ma & Bertschinger 1995) that describe the time evolution of the metric perturbations in the perturbed density field and the time evolution of the density fields in the perturbed spacetime for all the relevant particle species (e.g., photons, baryons, cold dark matter and massive neutrinos). The unperturbed energy density and pressure of massive neutrinos as well as their perturbed energy density and pressure, energy flux and shear stress in the  $k$ -space (see Ma & Bertschinger 1995 for their definitions) are specified once the full neutrino phase-space distribution function is known. The full massive neutrino phase-space distribution depends on the time, on the neutrino positions and momenta and

can be represented in the form (Ma & Bertschinger 1995, Ma 1999):

$$f(\mathbf{x}, \mathbf{q}, a) = f_0(\epsilon)(1 + \Psi(\mathbf{x}, \mathbf{q}, a)), \quad f_0(\epsilon) = \frac{g_s}{h_p^3} \frac{1}{e^{\epsilon/k_B T_\nu} + 1},$$

where  $\vec{q} = a\vec{p}$  is the neutrino comoving momentum,  $\vec{p}$  is the neutrino conjugate momentum,  $\epsilon = (q^2 + a^2 m_\nu^2)^{1/2}$  is the neutrino comoving energy,  $T_\nu = a^{-1} T_{\nu 0}$  is the neutrino temperature,  $T_{\nu 0} = (4/11)^{1/3} T_{\gamma 0} = 1.927(T_{\gamma 0}/2.7\text{K})$  K is the present neutrino temperature,  $T_{\gamma 0}$  being the present radiation temperature,  $g_s$  is the number of spin for degree of freedom, and  $h_P$  and  $k_B$  are the Planck and Boltzmann constants. In the above equation  $f_0(\epsilon)$  is a pure Fermi-Dirac distribution that depends only on the neutrino comoving energy and  $\Psi$  represents a perturbation term from this distribution depending on time and neutrino comoving momentum and position. In the actual version of the CMBFAST code (Seljak & Zaldarriaga 1996) the neutrino phase-space distribution, approximated by a pure Fermi-Dirac distribution, does not take into account the neutrino position dependence as indicated by the above equation. The inclusion of the full neutrino phase-space distribution can lead to the perturbations of the quantities related to the computation of the CMB angular power spectrum and matter transfer function.

The full neutrino phase-space distribution function for Cold + Hot Dark Matter (CHDM) models was computed before (Ma & Bertschinger 1994) by integrating the neutrino geodesic equations in the perturbed background spacetime. It was found a positive correlation between the neutrino *rms* velocities and the neutrino density fluctuations at a redshift  $z \sim 15$ , revealing the contribution of the perturbations to the Fermi-Dirac distribution.

In this paper we compute the initial full phase-space neutrino distribution function for CHDM and  $\Lambda$ CHDM models by using numerical simulations. We start from the HDM density fluctuation power spectrum with the normalization indicated by the analysis of the local cluster X-ray temperature function (Eke, Cole & Frenk 1996) and derive the initial neutrino phase-space distribution at each spatial wave number  $k$  by using the Zel'dovich

approximation (Zel’dovich 1970). The neutrino phase-space distributions obtained in this way are then implemented in the CMBFAST code as initial neutrino momentum distributions for the integration of the coupled linearized Einstein, Boltzmann and fluid equations in the  $k$ -space and the computation of CMB power spectra and matter transfer functions.

The cosmological parameters of the CHDM and  $\Lambda$ CHDM cosmological models considered in this paper and the initial conditions are presented in Section 2. The numerical simulation approach is described in Section 3. The CMB and matter power spectra obtained from numerical simulations are discussed and compared with those obtained in the case a pure Fermi-Dirac distribution in Section 4. In Section 5 we study the implications of the nonlinear bias factor and nonlinear effects of the matter density fluctuation power spectra to constrain the main cosmological parameters, when combined CMB and LSS data are taken into account. Finally, we discuss the results and draw out our conclusions in Section 6.

## 2. The initial conditions

### 2.1. Cosmological models

We present the computation of the full phase-space neutrino distribution function for two distinct CHDM and  $\Lambda$ CHDM models specified by the set of cosmological parameters given in Table 1, where we report also the parameters of the corresponding CDM (properly sCDM and  $\Lambda$ CDM) models [i.e. the sCDM ( $\Lambda$ CDM) model with the same parameter of the CHDM ( $\Lambda$ CHDM) model but with  $\Omega_\nu^{\text{sCDM}/\Lambda\text{CDM}} = 0$  and cold dark matter density parameter  $\Omega_c^{\text{sCDM}/\Lambda\text{CDM}} = \Omega_c^{\text{CHDM}/\Lambda\text{CHDM}} + \Omega_\nu^{\text{CHDM}/\Lambda\text{CHDM}}$ ]. For the CHDM and the  $\Lambda$ CHDM models we consider the contribution of one massless and two massive neutrino species while for the corresponding CDM models we consider the contribution of three massless neutrino species. We assume adiabatic perturbations and the presence of the scalar modes with the spectral

index  $n_s = 1$ , as predicted by the standard inflationary models (Guth & Pi 1981).

It is usual to describe the shape of the power spectrum of the density perturbations with the shape parameter  $\Gamma = \Omega_m h (\Omega_r / \Omega_{r0})^{-1/2}$  (Bardeen et al. 1986), where  $\Omega_r$  is the energy density parameter for all the relativistic particles and  $\Omega_{r0}$  corresponds to the standard model with photons and three massless neutrino species [ $\Omega_{r0} = 1.6813\Omega_\gamma$ ,  $\Omega_\gamma = 2.3812 \times 10^{-5} h^{-2} \Theta_{2.7}^4$ ,  $\Theta_{2.7} = T_{\gamma 0} / 2.7 \text{ K} \simeq 1.01$ ]. Observations require  $0.22 < \Gamma < 0.29$  (Peacock & Dodds 1994). The treatment of the cosmological models with HDM component requires the introduction of a second shape parameter,  $\Gamma_\nu = a^{1/2} \Omega_\nu h^2$ , that characterizes the effect of the neutrino free-streaming on the density fluctuation power spectrum (Ma 1996). Observations at the present time ( $z \simeq 0$ ) require  $\Gamma_\nu < 0.021$  (Gawiser 2000). The values the shape parameters  $\Gamma$  and  $\Gamma_\nu$  for our cosmological models are also reported in Table 1.

The choice of the cosmological models presented in Table 1 is motivated by observational evidencies. The CHDM model with two 2.4 eV neutrinos ( $m_\nu = 92h^2\Omega_\nu$  eV) was found in remarkably agreement with all the available LSS observations if  $h \simeq 0.5$  (Primack et al. 1995). The  $\Lambda$ CHDM model was found to be the best fit model of the current CMB experimental data combined with the Type 1a supernovae data when priors on  $H_0$  and  $\Omega_b$  are assumed (Tegmark & Zaldarriaga 2000).

□

## 2.2. Matter density fluctuation power spectrum and its normalization

The power spectrum of the matter density fluctuations is defined as (Bardeen et al. 1996):

$$\mathcal{P}(k, a) = \mathcal{A} k^{n_s} T(k, a)^2 \left( \frac{D(k, a)}{D_0(k)} \right)^2, \quad (1)$$

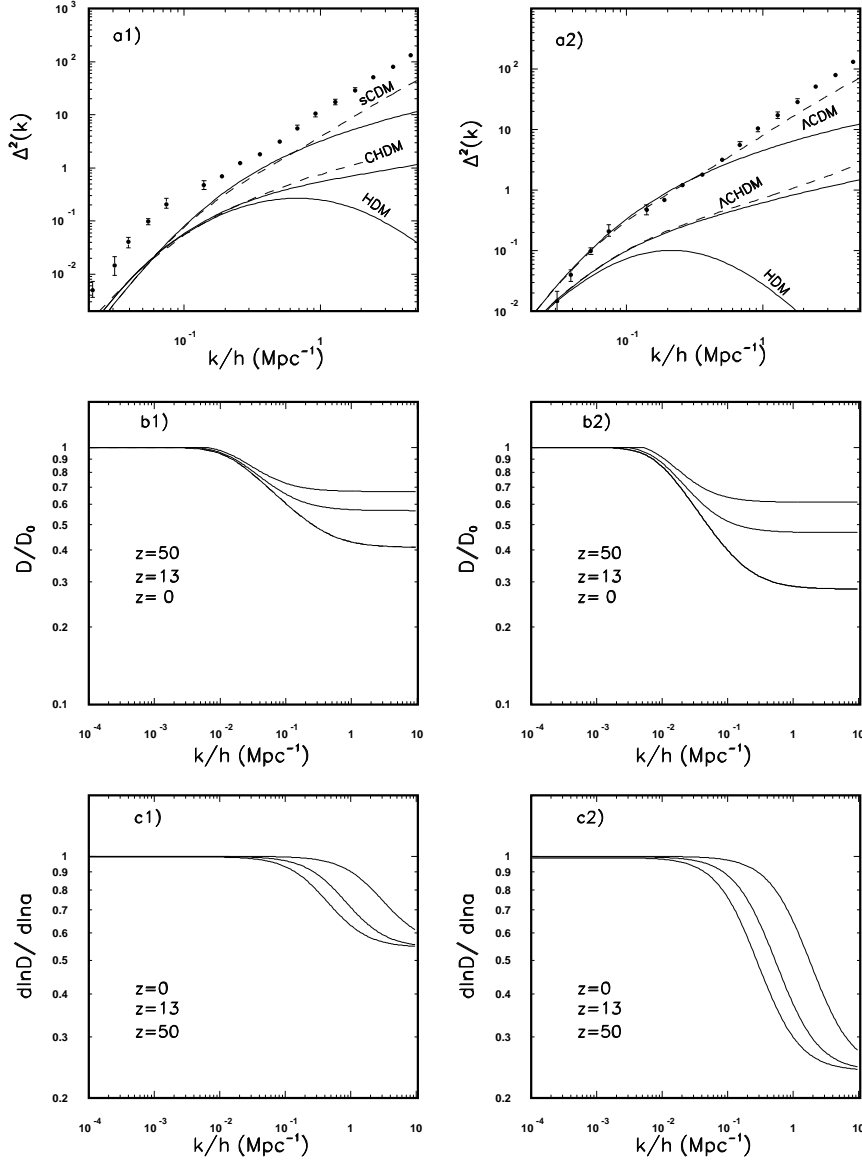


Fig. 1.— Panels a1) and a2): the weighted matter density fluctuation power spectra and the HDM component density fluctuation power spectra. The power spectra in the nonlinear regime are indicated with dashed lines. All the power spectra are normalized at  $\sigma_8$  and are computed at the present time. The experimental data points are derived from the APM galaxy survey. The evolution of the weighted matter density fluctuations and of the HDM component density fluctuation is shown in panels b1), c1) and b2), c2) respectively. Panels b1) and b2): the growth functions at some redshift values as function of the spatial wave number  $k$ . Panels c1) and c2): the corresponding growth rates at some redshift values as function of the spatial wave number  $k$ .

where  $\mathcal{A}$  is a normalization constant,  $k$  is the spatial wave number,  $T(k, a)$  is the matter transfer function and  $D(k, a)$  is the growth factor of the density perturbations assuming a value  $D_0(k) = D(k, a = 1)$  at the present time. We will refer in the following also to the growth rate, defined as  $f(k, a) = \text{dln}D/\text{dln}a$ .

The dimensionless power spectrum  $\Delta^2(k, a)$ , defined as the power per logarithmic interval in spatial frequency  $k$  (the power variance), is given by (Peebles 1980):

$$\Delta^2(k, a) = \frac{1}{2\pi^2} k^{n_s+3} \mathcal{P}(a, k). \quad (2)$$

The total matter density fluctuations contributed by the different matter components (baryons, cold dark matter particles, neutrinos) can be obtained by replacing  $T(k, a)$  in the equation (1) by the the weighted transfer function given by (Ma 1996):

$$T(k, a) = \frac{\Omega_b}{\Omega_m} T_b(k, a) + \frac{\Omega_c}{\Omega_m} T_{CDM}(k, a) + \frac{\Omega_\nu}{\Omega_m} T_\nu(k, a), \quad (3)$$

where  $T_b(k, a)$ ,  $T_{CDM}(k, a)$  and  $T_\nu(k, a)$  are the transfer functions of baryons, cold dark matter and neutrinos respectively. The growth factor determines the normalization of the amplitude of matter density fluctuations relative to the CMB one (Eisenstein, Hu & Tegmark 1008). For the sCDM and  $\Lambda$ CDM models the growth functions depend only on time (see Lahav et al. 1991, Carroll, Press & Turner 1992). The presence of neutrino free-streaming alters the growth rate and then for CHDM and  $\Lambda$ CHDM models the growth factors and the growth rates depend on the time and the spatial wave number  $k$  (Hu & Eisenstein 1998).

It is usual to define the normalization of the density fluctuation power spectrum as  $\sigma_8(a)$ , the linear *rms* mass fluctuations in a sphere of radius  $R=8h^{-1}\text{Mpc}$ , since the observed *rms* galaxy counts on this scale is about unit.  $\sigma_8(a)$  is related to the power spectrum  $\Delta^2(k, a)$  through:

$$\sigma_8(a) = \left[ \int_0^\infty \frac{dk}{k} \Delta_i^2(k, a) W^2(x) \right]^{1/2}, \quad (4)$$

where  $x = kR$  and  $W(x)$  is the window function. We take a top-hat window function of radius  $R=8h^{-1}\text{Mpc}$  in the real space:

$$W(x) = 3(\sin x - x \cos x)/x^3. \quad (5)$$

It is also possible to set the amplitude of the initial fluctuation spectrum to the measured CMB temperature fluctuations on large scales provided by the COBE/DMR experiment (Bunn & White 1997). However, the COBE normalization is sensitive to the power spectrum at  $k \simeq 10^{-3}h \text{ Mpc}^{-1}$ , that is not relevant for the galaxy clustering. Alternatively to the COBE normalization, the abundance of rich clusters can be used to fix the amplitude of the initial mass fluctuations close to the quasilinear scale (see also Jenkins et al. 1998 and Peacock 2000 for a discussion of the advantages of this kind of normalization).

We adopt the values of  $\sigma_8$  obtained by Eke, Cole & Frenk 1996 for CDM models as derived from the analysis of the local X-ray temperature function (for  $\sigma_8$  values obtained from slightly different analyses and consistent with these values see also White, Efstathiou & Frenk 1993, Viana & Liddle 1996, Pen 1997):

$$\begin{aligned} \sigma_8^{\text{CDM}} &= (0.52 \pm 0.04)\Omega_m^{-0.52+0.13\Omega_m} \quad (\text{flat models}) \\ \sigma_8^{\text{CDM}} &= (0.52 \pm 0.04)\Omega_m^{-0.46+0.1\Omega_m} \quad (\text{open models}) \end{aligned} \quad (6)$$

For the cosmological models involving a HDM component, the value of  $\sigma_8$  is given by (Ma 1996):

$$\sigma_8 = \sigma_8^{\text{CDM}} \times \sigma_8^{\text{HDM}}, \quad (7)$$

where  $\sigma_8^{\text{HDM}}$  and  $\sigma_8^{\text{CDM}}$  are the normalizations for the HDM model and the corresponding CDM model respectively. For the purpose of this paper we take  $\sigma_8^{\text{CDM}}$  as given by the equations (6) and  $\sigma_8^{\text{HDM}}$  as obtained in the COBE normalization, as computed by the CMBFAST code. The values of  $\sigma_8$  and  $\sigma_8^{\text{HDM}}$  for the cosmological models considered here are also reported in Table 1. For comparison, we present also the values of  $\sigma_8^c$  derived when

$\sigma_8^{\text{CDM}}$  is obtained in the COBE normalization. One can see that while for  $\Lambda\text{CHDM}$  models the  $\sigma_8$  values derived on the basis of these two normalizations are almost identical, they differ by a factor of about two in the case of CHDM models.

We also indicate in Table 1 the values of the free-streaming wave number  $k_{fs}$  and of the wave number  $k_{nl}$  at which the nonlinear effects become important (Peacock & Dodds 1996):

$$\begin{aligned} k_{fs} &\approx 0.026 \left( \frac{m_\nu}{1\text{eV}} \right)^{1/2} \Omega_m^{1/2} \text{hMpc}^{-1}, \\ k_{nl} &= \left[ \frac{((n_{\text{eff}} + 1)/2)!}{2} \right]^{1/(n_{\text{eff}} + 3)} \frac{\sqrt{10}}{R} \text{hMpc}^{-1}, \quad n_{\text{eff}}(k_L) = \frac{d \ln P(k)}{d \ln k} (k = k_L/2), \end{aligned} \quad (8)$$

where  $k_L$  is the linear wave number and  $n_{\text{eff}}(k_L)$  is the effective spectral index of the power spectrum.

Figure 1 presents the weighted matter density fluctuation power spectra and the HDM component density fluctuation power spectra for the considered cosmological models, with the transfer functions given by the CMBFAST code. All the matter power spectra are normalized at  $\sigma_8$  as given by the equations (6)-(7) and are computed at the present time.

The nonlinear matter density fluctuation power spectra (dashed lines in Figure 1) are computed with the formalism of Peacock & Dodds 1996 by using the appropriate linear growth rate functions given by the ratio between the power spectrum of each cosmological model and the power spectrum of the corresponding CDM model (Ma 1996) calculated with the linear growth factor of the CDM model given by (Peebles 1980):

$$g(\Omega_m, \Omega_\Lambda) = \frac{D}{a} = \frac{5\Omega_m}{2} \int_0^1 \frac{da}{a^3 H(a)^3}, \quad (9)$$

where  $\Omega_K = 1 - \Omega_m - \Omega_\Lambda$  is the curvature density parameter and  $H(a) = (\Omega_m a^{-3} + \Omega_K a^{-2} + \Omega_\Lambda)^{1/2}$  is the Hubble expansion rate normalized to unit at the present time. We test the validity of Peacock & Dodds formula for  $k/h \sim 5 \text{ Mpc}^{-1}$ , finding a very good agreement with the analytical approximation to the nonlinear power spectra for CHDM models obtained by Ma (1998).

We present also in Figure 1 the corresponding growth functions and growth rates for the considered cosmological models computed at some representative epochs.

### 3. N-body simulations

We obtain the initial neutrino phase-space distributions at each spatial wave number  $k$  through numerical simulations based on the standard particle-mesh (PM) method (Efstathiou & Eastwood 1981, Hockney & Eastwood 1981) usually used to set the initial conditions for the nonlinear evolution of the large-scale structure (see Jenkins et al. 1998 and the references therein).

The initial neutrino positions and velocities are generated from the HDM matter density fluctuation power spectrum with the normalization given by the equation (6)-(7) by using Zel’dovich approximation (Zel’dovich 1970). According to the Zel’dovich approximation, the perturbed comoving position of a particle  $\vec{r}(\vec{r}_0, a)$  and its peculiar velocity  $\vec{v}(\vec{r}_0, a)$  are related to the fluctuations of the density field  $\delta\rho_{HDM}(\vec{r}_0, a, k)$  through:

$$\begin{aligned} \vec{r}(\vec{r}_0, k, a) &= \vec{r}_0 + D(k, a)\vec{d}(\vec{r}_0), & \vec{v}(\vec{r}_0, k, a) &= \dot{D}(k, a)\vec{d}(\vec{r}_0), \\ \vec{\nabla}\vec{d}(\vec{r}_0) &= D^{-1}(k, a)\delta\rho_{HDM}(\vec{r}_0, k, a), \end{aligned} \quad (10)$$

where  $\vec{r}_0$  is the coordinate corresponding to the unperturbed comoving position and  $\vec{d}(\vec{r}_0)$  is the displacement field. In the simulations we use the set of equations (10) to compute the perturbed neutrino comoving positions, the neutrino peculiar velocities and the displacement of the density fields for each wave number  $k$  at the present time. We assign to each neutrino a momentum according to the growth function, when the power of each mode is randomly selected from a Gaussian distribution with the mean accordingly to the power spectrum of the HDM component (Hoffman & Ribak 1991, Ganon & Hoffman 1993, Bertschinger 1995), and add a thermal momentum randomly drawn from a Fermi-Dirac

distribution:

$$f(q_0) \sim \frac{q_0^2}{e^{q_0} + 1}, \quad q_0 = \mathcal{M}_\nu v/c \quad \text{and} \quad \mathcal{M}_\nu = \frac{m_\nu c^2}{k_B T_{\nu_0}}, \quad (11)$$

where  $\vec{v}$  is the neutrino velocity and  $c$  is the speed of light. We performed simulations with  $10 \times 32^3$ ,  $10 \times 64^3$  and  $10 \times 128^3$  particles. The neutrinos with identical masses are randomly placed on  $32^3$ ,  $64^3$  and  $128^3$  grids, 10 per grid point, with comoving spacing  $r_0$  in the range  $(0.5 - 5) \text{ h}^{-1} \text{ Mpc}$ . We verify the convergence of the results with the variation of the number of particles and the comoving spacing. The results presented here are obtained from ten simulations with  $10 \times 128^3$  neutrinos and a comoving spacing of  $r_0=0.5 \text{ Mpc}$ . This large number of particles ensures enough statistics for the computation of the phase-space distributions, while this comoving spacing was found to give the minimum variance of the likelihood distribution functions presented in Figure 4. In the computation of the set of equation (10) we consider only the growing modes, the nonlinear power spectrum up to  $k_{max} = 6.28 \text{ h Mpc}^{-1}$  and neglect the contribution of the redshift distortions on the power spectrum.

The neutrino momentum field obtained at each wave number  $k$  was sampled in fixed equispaced points (we use here  $N_{q_{max}}=50$ ) and normalized to the neutrino total number ( $N_{part} = 10 \times 128^3$  in the current simulation).

Figure 2 shows (left panels) the contour plots of the constant particle probabilities in the  $\delta q - \delta \rho_{HDM}$  plane, where  $\delta q = q_i(k) - \langle q(k) \rangle$ ,  $q_i(k)$  being the peculiar neutrino momentum and  $\langle q(k) \rangle$  the bulk neutrino momentum of the lattice:

$$\langle q(k) \rangle = \frac{1}{N_{part}} \sum_i q_i(k). \quad (12)$$

We also show (right panels) the momentum distribution functions obtained from numerical simulations (continuous line) compared with the thermal momentum distribution function (dashed line). We find a displacement of the bulk neutrino momentum towards higher

values for the same wave number when  $\sigma_8$  increases. Also, for the same value of  $\sigma_8$ , the bulk neutrino momentum is displaced towards smaller values with the increasing of the wave number, reflecting the  $k$ -dependence of the growth function. The dominant effect is given by the variation of the  $\sigma_8$  value.

#### 4. The CMB power spectrum from numerical simulations

The neutrino momentum distributions obtained from numerical simulations at each wave number  $k$  are used as initial neutrino phase-space distributions in the CMBFAST code for the integration of the Boltzmann, Einstein and fluid equations. As usual, the neutrino comoving energy is then  $E = (q^2 + a^2 \mathcal{M}_\nu^2)^{1/2}$  (Ma & Bertschinger 1995), where  $q$  is the neutrino comoving momentum. Following the same procedure implemented in the CMBFAST code, we compute in synchronous gauge the perturbations of the energy density, pressure, energy flux and shear stress, truncating the Boltzmann hierarchies for massive neutrinos at  $l_{max} = 50$  for every value of  $q$ , obtaining a relative accuracy in the estimation of the CMB power spectrum better than  $\simeq 10^{-3}$  (Popa et al. 2000).

Figure 3 presents the evolution with the scale factor of the energy density parameters of different components and of their density perturbations, and of the neutrino shear stress and energy flux obtained for the CHDM model for the neutrino phase-space distribution function modelled as a Fermi-Dirac distribution (continuous lines) or obtained from the numerical simulations when the normalization of the matter power spectrum is  $\sigma_8 = 0.3$  (dashed lines) or  $\sigma_8 = 0.81$  (dotted-dashed lines). One can see that while the time evolution of the various energy density components obtained from numerical simulations are not changed, their perturbations as well as the neutrino shear stress and energy flux differ from those obtained in the case of a pure Fermi-Dirac distribution. As it was mentioned before, the full neutrino phase-space distribution depends also on the neutrino position, leading to

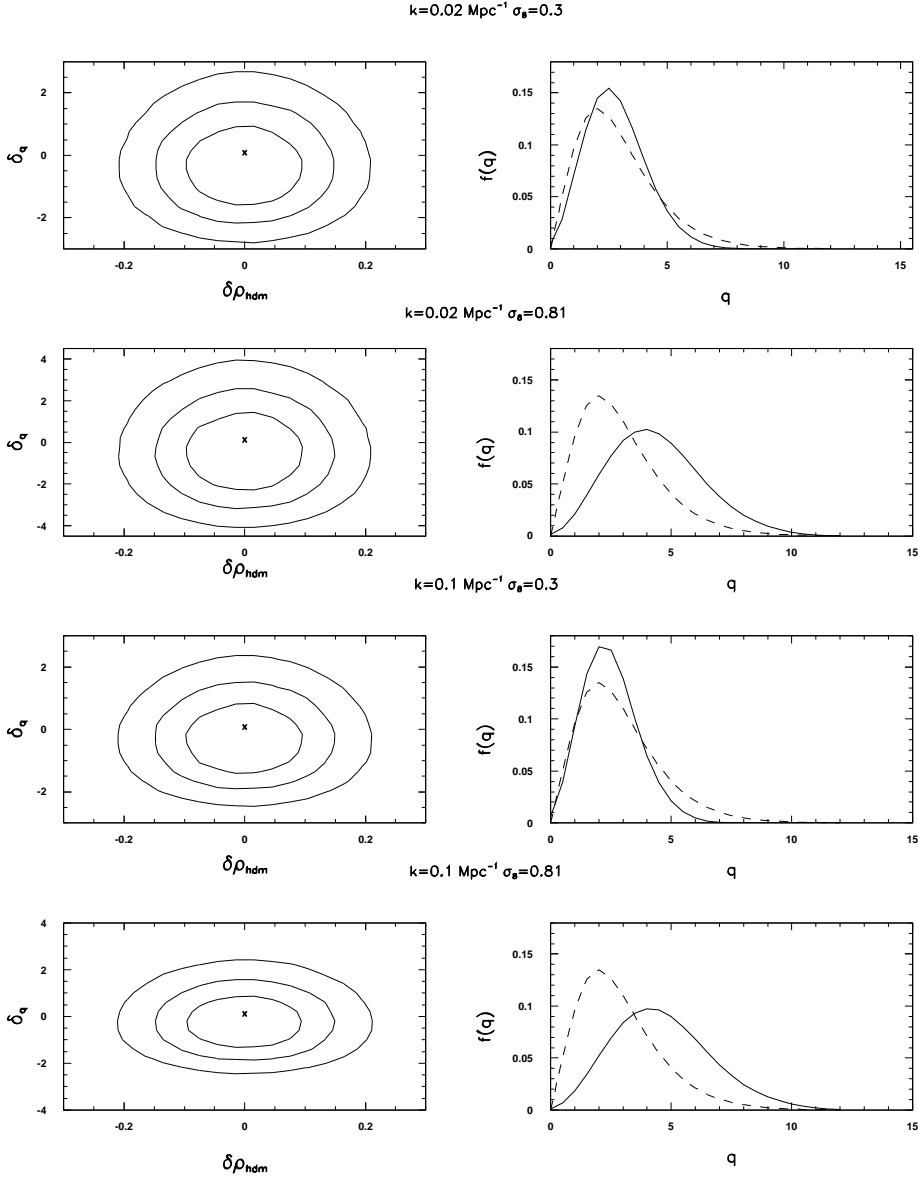


Fig. 2.— Left panels: the contour plots of constant particle probabilities in the  $\delta q - \delta \rho_{HDM}$  plane (see also the text). From exterior to interior the contours correspond to: 0.75, 0.5 and 0.25 probability. Right panels: the momentum distribution functions obtained from numerical simulations (continuous line) and the thermal momentum distribution function (dashed line). These plots refer to the case of the CHDM cosmological model.

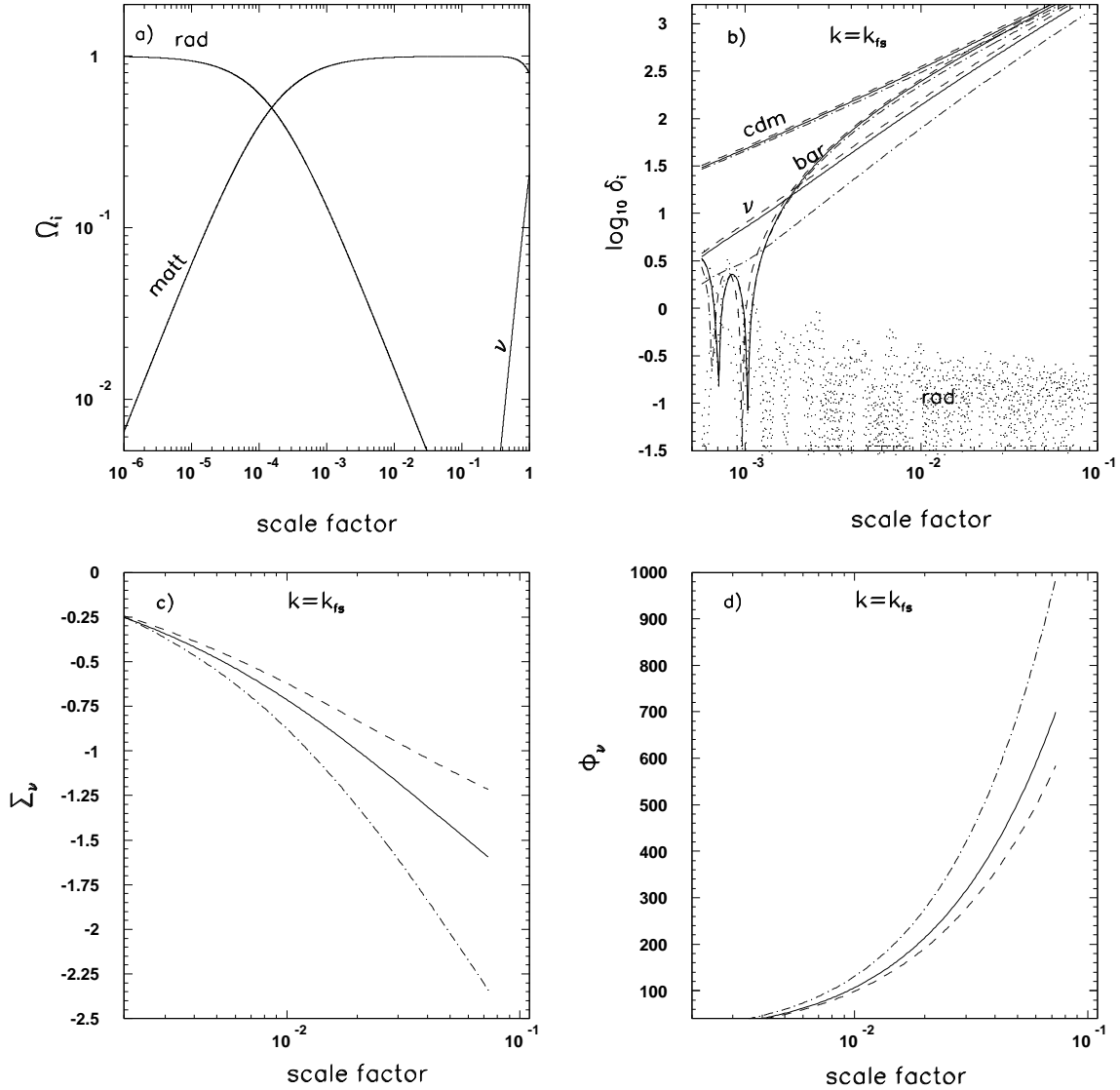


Fig. 3.— Panel a): the time evolution of the energy density of the different components (see also the text). Panel b): the time evolution of energy density perturbations for different components when the neutrino phase-space distribution is a Fermi-Dirac distribution (continuous line) or it is obtained from numerical simulations with  $\sigma_8 = 0.3$  (dashed line) or with  $\sigma_8 = 0.81$  (dotted-dashed line). Panel c): the time evolution of the neutrino shear stress when the neutrino phase-space distribution is a Fermi-Dirac distribution (continuous line) or it is obtained from numerical simulations with  $\sigma_8 = 0.3$  (dashed line) or with  $\sigma_8 = 0.81$  (dotted-dashed line). Panel d): the same as in the panel c) but for neutrino energy flux. The distributions presented in panels b) c) and d) are obtained at  $k = k_{fs}$ . All the plots refer to the CHDM cosmological model.

perturbations of the pure Fermi-Dirac distribution,  $f(\vec{x}, q, t) = f_0(q)[1 + \Psi(\vec{x}, q, t)]$ , where  $f_0(q)$  is the pure Fermi-Dirac distribution. These perturbations are reflected by the time evolution of the quantities presented in Figure 3.

Figure 4 presents the CMB anisotropy power spectra obtained from numerical simulations for different normalizations of the matter density fluctuations power spectra, for the CHDM (panel a1)) and the  $\Lambda$ CHDM models (panel b1)). Each power spectrum is obtained by averaging the power spectra from ten simulations with  $10 \times 128^3$  particles and normalized to COBE/DMR (Bunn & White 1997). We also show in Figure 4 the likelihood dependence on  $\sigma_8$  for the CHDM model (panel a2)) and  $\Lambda$ CHDM model (panel b2)). For each case the target power spectrum is the corresponding power spectrum given by the CMBFAST code normalized to the COBE/DMR data. We found at  $1 - \sigma$  level the following values for  $\sigma_8$ :

$$\begin{aligned} \sigma_8 &= 0.34 \pm 0.09 \quad \text{for CHDM} \\ \sigma_8 &= 0.3 \pm 0.07 \quad \text{for } \Lambda\text{CHDM.} \end{aligned}$$

These values of  $\sigma_8$  show that the CMB power spectrum in COBE normalization is well recovered when the matter density fluctuation power spectrum is normalized to the cluster abundance data, as indicated in the Table 1. The results presented in Figure 4 show that the relative amplitude between the CMB temperature fluctuations and the matter density fluctuations normalized to COBE/DMR is well defined by the CDM component with the normalization indicated by the abundance of the rich clusters at the present time. This result confirms the predictions of the structure formation theories in which the CDM driven by the adiabatic fluctuations leads to the formation of the CMB anisotropy and large scale structure (see, e.g., Dodelson, Gates & Turner 1996). Figure 5 presents the time evolution of the bias factor  $b_I = 1/\sigma_8$  (panel a)) and of the parameter  $\Omega_m^{0.6}/b_I$  (panel b)), usually measured from the peculiar velocity data, obtained for the CHDM and the  $\Lambda$ CHDM model.

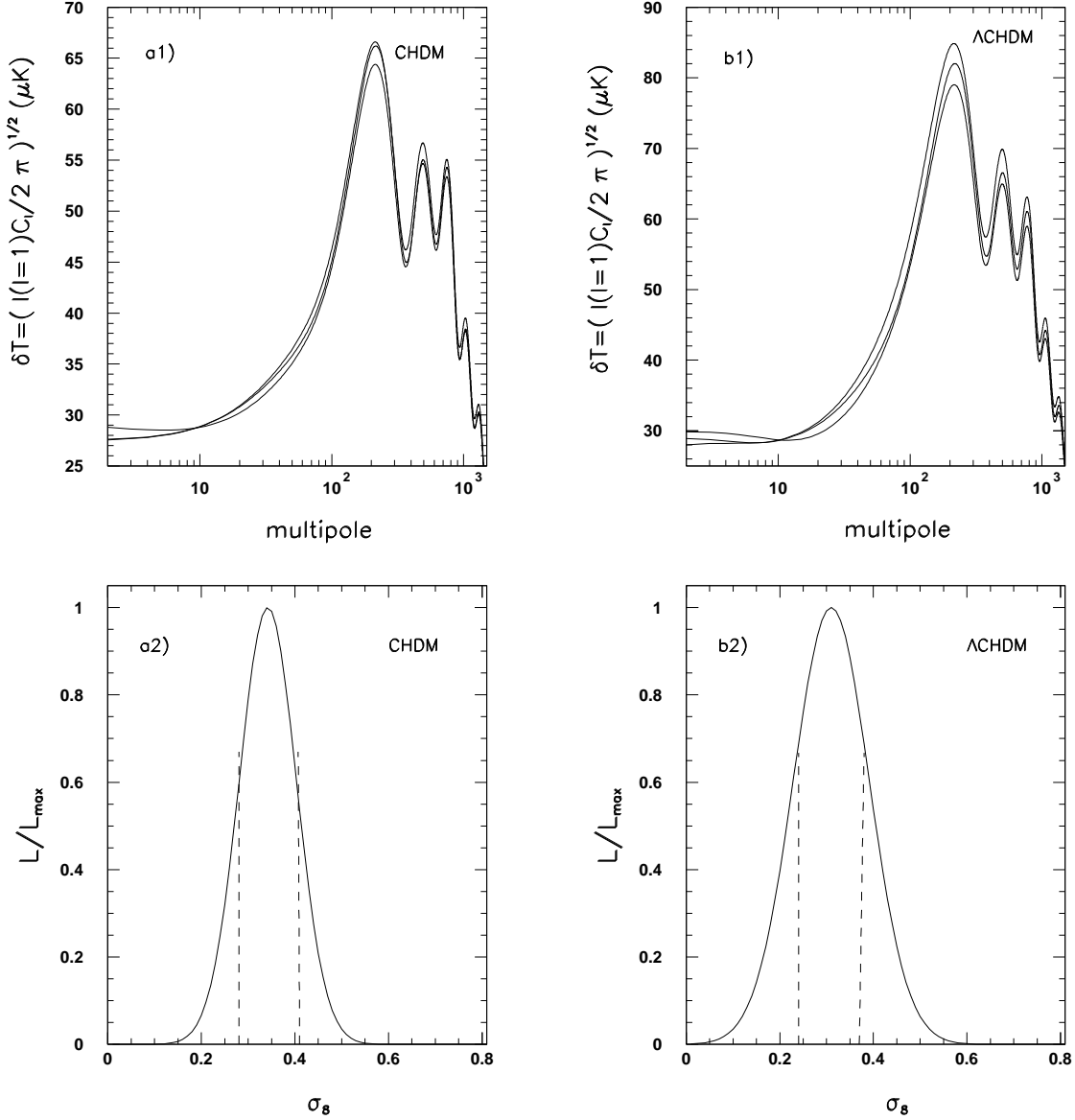


Fig. 4.— The CMB anisotropy power spectra obtained from numerical simulations for CHDM model (panel a1)) and  $\Lambda$ CHDM model (panel a2)) for different values of  $\sigma_8$ . From the top to the bottom (at the first Doppler peak):  $\sigma_8=0.2, 0.3, 0.5$ . The likelihood dependence on  $\sigma_8$  obtained in CHDM model (panel b1)) and  $\Lambda$ CHDM model (panel b2)). All the reported power spectra are obtained averaging over ten simulations and are normalized to COBE/DMR data.

For both models the normalization at the present time is given by the equations (6)-(7).

## 5. Cosmological parameter determination from CMB and LSS data in $\Lambda$ CHDM cosmologies

The results obtained in the previous section show that the relative bias between the CMB anisotropy power spectrum and the matter density fluctuation power spectrum in the COBE/DMR normalization is given by the CDM component with the normalization obtained from the abundance of the rich clusters at the present time. This confirms the idea to jointly use the cosmological information contained in the CMB power spectrum and in the matter power spectrum to constrain degenerated sets of cosmological parameters.

There are few factors that alter the relative amplitude between CMB temperature fluctuations and the underlying mass density fluctuations: the growth rate of perturbations depends upon  $\Omega_m$  and  $\Omega_\Lambda$  and implicitly upon  $\Omega_K$  (see equation (9)). The degeneracy between  $\Omega_\Lambda$  and  $\Omega_K$  leads to an indeterminacy of the Hubble constant (Efstathiou & Bond 1999):

$$h = (\omega_m + \omega_\Lambda + \omega_k)^{1/2}, \quad (13)$$

where  $\omega_i = \Omega_i h^2$  are the physical densities of the relevant components. The CMB anisotropy measurements can constrain  $\omega_m = \omega_b + \omega_c + \omega_\nu$  and  $\omega_b$  from the morphology of the Doppler peaks.

On the other hand, the observed power spectrum in the redshift space differs from the theoretical power spectrum of mass fluctuations because of the nonlinear evolution, redshift-space mapping and the bias. For the purpose of this paper we consider a scale-independent bias factor  $b_I = 1/\sigma_8$ , and compute the effects of the nonlinear evolution by using the Peacock & Dodds formula (see Section 2). Following Feldman, Kaiser & Peacock (1994) we

Table 1: Parameters of the considered cosmological models and other relevant quantities ( $\Omega_m = \Omega_b + \Omega_c + \Omega_\nu$ ).

Model	$\Omega_b$	$\Omega_c$	$\Omega_\nu$	$\Omega_\Lambda$	h	$\Gamma$	$\Gamma_\nu$	$\sigma_8^{\text{HDM}}$	$\sigma_8$	$\sigma_8^c$	$k_{fs}$ ( $\text{Mpc}^{-1}$ )	$k_{nl}$ ( $\text{Mpc}^{-1}$ )
CHDM	0.05	0.75	0.2	0	0.5	0.58	0.05	0.68	$0.36 \pm 0.02$	0.81	0.06	0.46
$\Lambda$ CHDM	0.03	0.2	0.1	0.67	0.65	0.25	0.04	0.33	$0.32 \pm 0.02$	0.31	0.03	0.35
sCDM	0.05	0.95	0	0	0.5	0.5	-	-	$0.52 \pm 0.03$	1.17	-	0.46
$\Lambda$ CDM	0.03	0.3	0	0.67	0.65	0.21	-	-	$0.88 \pm 0.06$	0.92	-	0.35

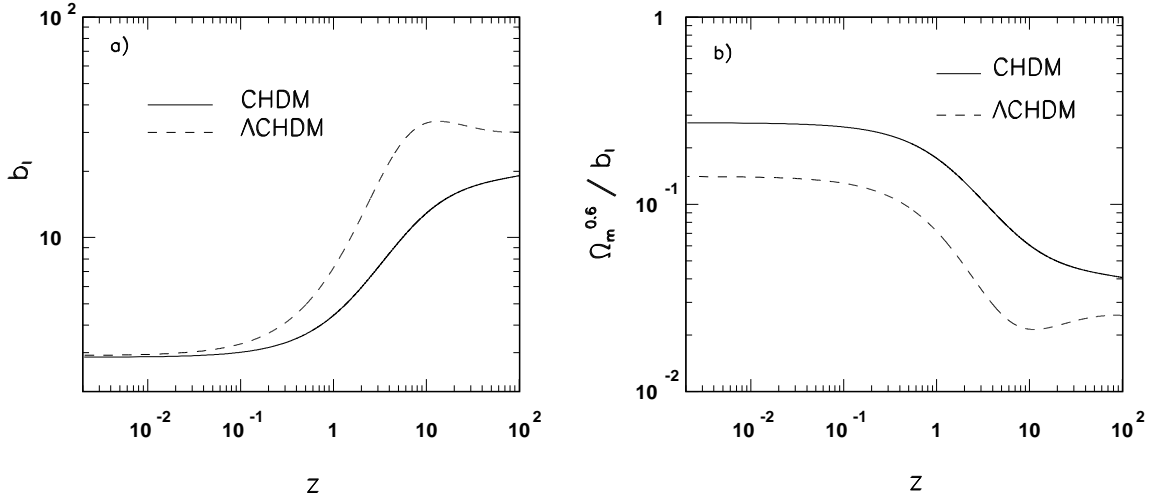


Fig. 5.— The redshift dependence of the bias factor  $b_I$  (panel a)) and of the parameter  $\Omega_m^{0.6}/b_I$  (panel b)) obtained for the CHDM and the  $\Lambda$ CHDM models, when the CDM component at the present time is normalized to the cluster abundance data (see also the text).

correct the nonlinear power spectrum of mass fluctuations for redshift distortions. On large scales the redshift distortions cause a linear increase of the power given by:

$$\mathcal{P}(k) \rightarrow \mathcal{P}(k) \left[ \frac{\Omega_m^{0.6}}{3b_I} + \frac{\Omega_m^{1.2}}{5b_I^2} \right]. \quad (14)$$

On small scales the redshift distortions cause:

$$\mathcal{P}(k) \rightarrow \mathcal{P}(k) \frac{\sqrt{\pi} \operatorname{erfc}(k\sigma)}{2} \frac{1}{k\sigma}, \quad (15)$$

where  $\sigma$  measures the spatial *rms* distortion and  $\operatorname{erfc}$  is the complementary error function. The typical values of  $\sigma$ , indicated by the *rms* small scale velocity measurements (Feldman, Kaiser & Peacock 1994), is of few  $h^{-1}\text{Mpc}$ . The indeterminacy of  $h$  causes the movement of the matter density power spectrum in the redshift space, changing the normalization scale, the neutrino free-streaming scale  $k_{\text{fs}}$ , and the scale  $k_{\text{nl}}$  at which the nonlinear effects become important (see Section 2).

The relative normalization between the CMB and matter power spectra depends also on  $\omega_m$ . While  $\omega_m$  and  $\omega_b$  can be constrained from the CMB Doppler peak distribution, the strong dependence of the matter power spectrum on  $\omega_\nu$  at intermediate and small scales constrains  $\omega_c$ .

The spectral index of the scalar modes  $n_s$ , the spectral index of the tensorial modes  $n_t$ , the ratio T/S between tensorial and scalar contributions as well as the reionization effects (an optical depth to the last scattering  $\tau \neq 0$ ) affect also the relative bias between the CMB temperature fluctuations and the matter density fluctuations. Within the CMB polarization data  $n_t$ ,  $T/S$  and  $\tau$  can well be constrained, while the indeterminacy of most of the cosmological parameters is reduced (see, e.g., Zaldarriaga, Spergel & Seljak 1997, Zaldarriaga & Seljak 1997).

We compute the precision at which the fundamental cosmological parameters could be extracted from the combined CMB anisotropy and LSS data given by PLANCK and

SDSS, taking into account the dependence of the CMB and matter power spectrum on all the factors enumerated before. The previous papers on the parameter estimation from CMB and LSS data (see, e.g., Scott et al. 1995, Bond, Jaffe & Knox 1998, Lineweaver 1998, Webster et al. 1998, Wang et al. 1998, Eisenstein, Hu & Tegmark 1999b) in general consider the normalization to the COBE data, neglecting the cosmological contribution to the estimation of the cosmological parameters of the nonlinear effects and redshift distortions.

We use the Fisher matrix approximation to compute the errors on the estimates of the cosmological parameters (see, e.g., Efstathiou & Bond 1999, Popa et al. 1999) for the experimental specifications of PLANCK and SDSS. In this case, the Fisher matrix elements are the sum of two terms, accounting for the Planck measurements of the CMB anisotropy and polarization and the galaxy power spectrum as derived from SDSS (Tegmark 1997):

$$F_{ij} = F_{ij}^{\text{Planck}} + F_{ij}^{\text{SDSS}}. \quad (16)$$

The minimum error that can be obtained on a parameter  $s_i$  when we need to determine all parameters jointly, is given by:

$$\delta s_i = \sqrt{F_{ii}^{-1}}, \quad (17)$$

depending on the experimental specifications, the target model and the class of considered cosmological models. If both anisotropy and polarization power spectra are used, the first Fisher information matrix term is given by (Zaldarriaga & Seljak 1997, Zaldarriaga 1997):

$$F_{ij}^{\text{Planck}} = \sum_l \sum_{X,Y} \frac{\partial C_{Xl}}{\partial s_i} C_{ov}^{-1}(\hat{C}_{Xl}, \hat{C}_{Yl}) \frac{\partial C_{Yl}}{\partial s_j}, \quad (18)$$

where  $X$  and  $Y$  stands for  $T$ ,  $E$ ,  $C$  and  $B$  power spectra and  $C_{ov}^{-1}$  is the inverse of the covariance matrix. The PLANCK experimental parameters and the procedure used to compute the Fisher matrix term given by the equation (18) are described in Popa et al. (2000); in particular, we consider here, for simplicity, the PLANCK “cosmological channels” only (between 70 and 217 GHz) and neglect the foreground contamination.

The second term of the Fisher information matrix in equation (16) is given by (Tegmark 1997):

$$F_{ij}^{\text{SDSS}} = 2\pi \int_{k_{\min}}^{k_{\max}} \frac{\partial \ln P(k)}{\partial s_i} w(k) \frac{\partial \ln P(k)}{\partial s_j} d \ln k, \quad (19)$$

where  $k_{\min}$ ,  $k_{\max}$  are the minimum and maximum wave number used to compute the matter density fluctuation power spectra (we take a fixed  $k_{\min} = 10^{-4} \text{hMpc}^{-1}$  while the value of  $k_{\max}$  can vary) and  $w(k)$  is the selection function for the Bright Red Galaxy (BRG) sample of the SDSS. According to Tegmark (1997):

$$w(k) = \frac{V_{\text{eff}}(k)}{\lambda^3}. \quad (20)$$

Here  $V_{\text{eff}}(k)$  is the effective volume of the BRG sample used for measuring the power at the wave number  $k$  corresponding to the wavelength  $\lambda = 2\pi/k$ :

$$V_{\text{eff}} = \int \left[ \frac{\bar{n}(\vec{r}) \mathcal{P}(k)}{1 + \bar{n}(\vec{r}) \mathcal{P}(k)} \right] d^3 r, \quad (21)$$

where  $\bar{n}(\vec{r})$  is the selection function of the survey that gives the expectation value of the number density of galaxies. We consider the BRG sample of SDSS volume-limited at  $1000 \text{h}^{-1} \text{Mpc}$ , containing  $10^5$  galaxies (Tegmark 1997) with a bias factor given by the equations (6)-(7) and  $\bar{n}(\vec{r})$  is the expectation value of the Poisson distribution.

The fiducial model is the flat  $\Lambda$ CHDM model with:  $\Omega_b = 0.047$ ,  $\Omega_c = 0.233$ ,  $\Omega_\Lambda = 0.67$ ,  $\Omega_\nu = 0.05$  ( $m_\nu = 2.1 \text{eV}$ ),  $H_0 = 65 \text{ Km s}^{-1} \text{ Mpc}^{-1}$ , one relativistic neutrino flavor,  $N_{\text{rel}} = 1$ , and two massive neutrino flavors,  $\Gamma = 0.25$ ,  $\Gamma_\nu = 0.021$ ,  $\sigma_8 = 0.42$ ,  $k_{\text{fs}} \approx 0.03 \text{Mpc}^{-1}$  and  $k_{\text{nl}} \approx 0.32 \text{Mpc}^{-1}$ . We assume primordial adiabatic perturbations, the presence of the scalar modes with the scalar spectral index  $n_s = 1$ , the contribution of the tensorial modes (gravitational waves) with the spectral index  $n_t = -0.09$ , a tensor-to-scalar ratio  $T/S=0.1$  and an optical depth to the last scattering  $\tau = 0$ . The independent parameters in our computation are:  $\omega_b$ ,  $\omega_c$ ,  $\omega_\nu$ ,  $\omega_\Lambda$ ,  $n_s$ ,  $n_t$ ,  $T/S$ ,  $\tau$  and  $\sigma$ . We fix  $\sigma_8$  at the value given by the equations (6)-(7) for each corresponding cosmological model and consider a linear bias  $b_I = 1/\sigma_8$ .

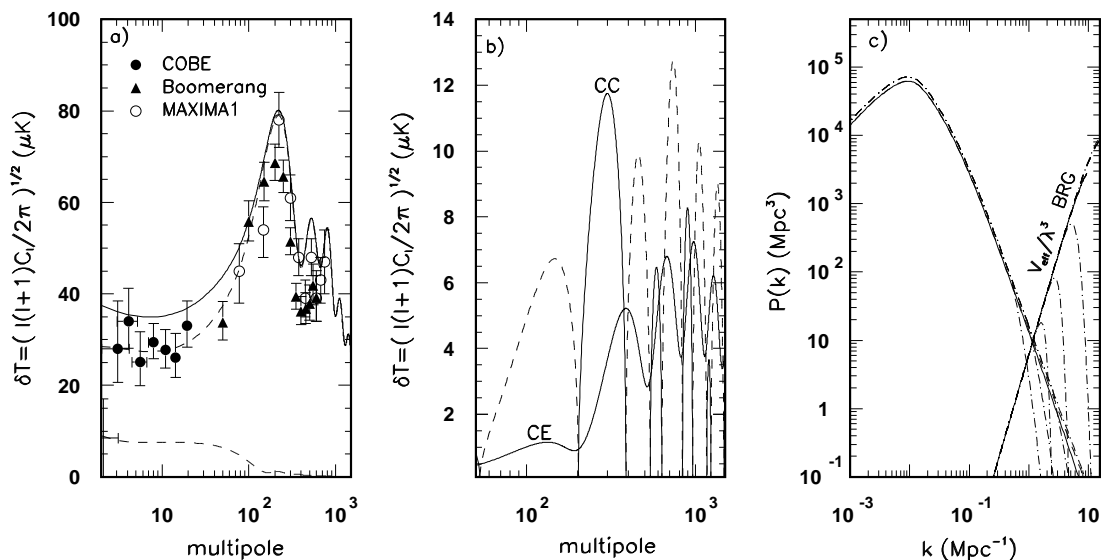


Fig. 6.— Panel a): the CMB anisotropy power spectrum of the fiducial model (continuous line) and its decomposition into scalar and tensorial contributions (dashed lines), compared with the CMB anisotropy experimental data from COBE, Boomerang and MAXIMA1. Panel b): the polarization power spectra of the fiducial model for E-channel (continuous line) and cross-correlation C-channel (dashed and dotted-dashed lines; the dotted-dashed line represents the negative part of the power spectrum). Panel c): the matter fluctuations power spectrum of the fiducial model and  $V_{eff}(k)/\lambda^3$  obtained for the fiducial model and the experimental specifications of the BRG sample of SDSS. The solid curves are for the linear regime, the dashed curves are obtained for the nonlinear regime and the dotted-dashed curves are obtained when both nonlinear effects and redshift distortions are considered, for few choices of  $\sigma$ ; from top to bottom  $\sigma=0,0.2,0.5,1 h^{-1}\text{Mpc}$  (see also the text). The power spectra are computed at the present time and normalized according to the equations (6)-(7).

Panel a) of Figure 6 presents the CMB anisotropy power spectrum of the fiducial model (continuous line) and its decomposition into scalar and tensorial contributions (the dashed lines) compared with the CMB anisotropy experimental data from COBE, Boomerang and MAXIMA1. Panel b) shows the polarization power spectra of the fiducial cosmological model. Panel c) of Figure 6 presents the matter fluctuations power spectrum of the fiducial model and the effective volume of the BRG sample of SDSS obtained for the fiducial model. The solid curves are for the linear regime, the dashed curves are obtained for the nonlinear regime and the dash-dotted curves are obtained when both nonlinear effects and redshift distortions are considered. For the last case we plot the matter power spectrum and  $V_{eff}/\lambda^3$  for few choices of parameter  $\sigma$  in the equation (15). We take for the fiducial model  $\sigma \approx 0$ . This makes the correction factor in equation (15) of order unit for the fiducial model.

Figure 7 presents the  $1 - \sigma$  errors on the estimates of the cosmological parameters that can be obtained by SDSS alone as a function of  $k_{max}$ . The solid curves are obtained assuming the linear matter power spectra in equations (19)-(21). The dashed curves are obtained when the nonlinear effects and the redshift distortions on the matter power spectra are taken into account.

For the computation of the Fisher matrix elements given by the equation (19) we take two-sided derivatives of  $\mathcal{P}(k)$  considering a step size of  $\Delta s_i \approx 5\%$ .

Parameters as  $n_t$ , T/S and  $\tau$ , not considered in Figure 7, do not affect the matter power spectrum for the SDSS experimental specifications considered here. The results presented in Figure 7 show that the SDSS power spectrum information alone can give modest constraints on most of the cosmological parameters in both linear and nonlinear regime, strongly dependent on the choice of  $k_{max}$  value.

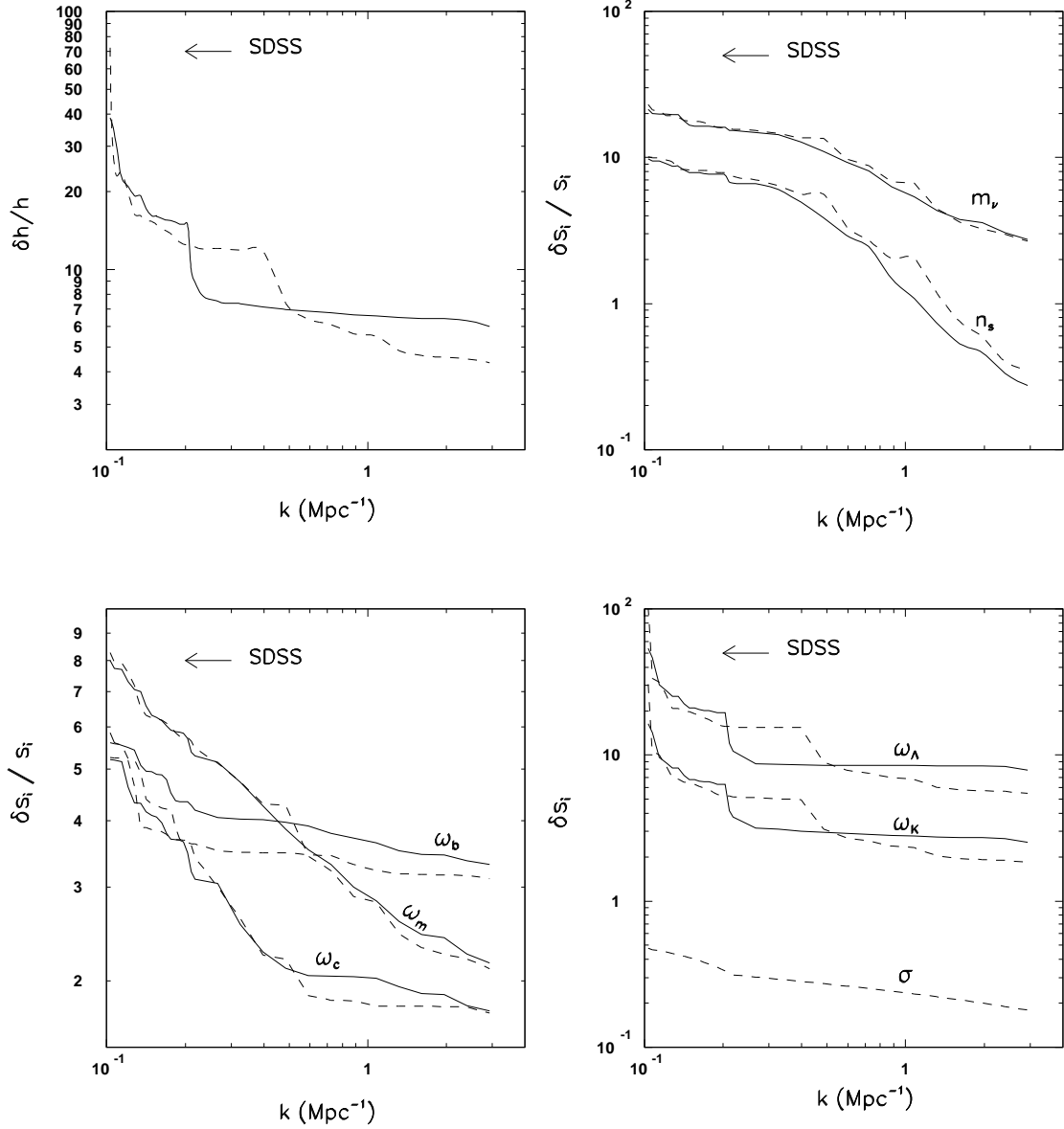


Fig. 7.—  $1-\sigma$  errors on the estimates of the cosmological parameters that can be obtain by SDSS alone from the linear matter power spectrum (continuous lines) and from the matter power spectrum corrected for nonlinear effects and redshift distortions (dashed lines) as function of  $k_{max}$ . The maximum  $k$  accessible to SDSS ( $\sim 0.3 \text{ Mpc}^{-1}$ ) is indicated by the arrow.

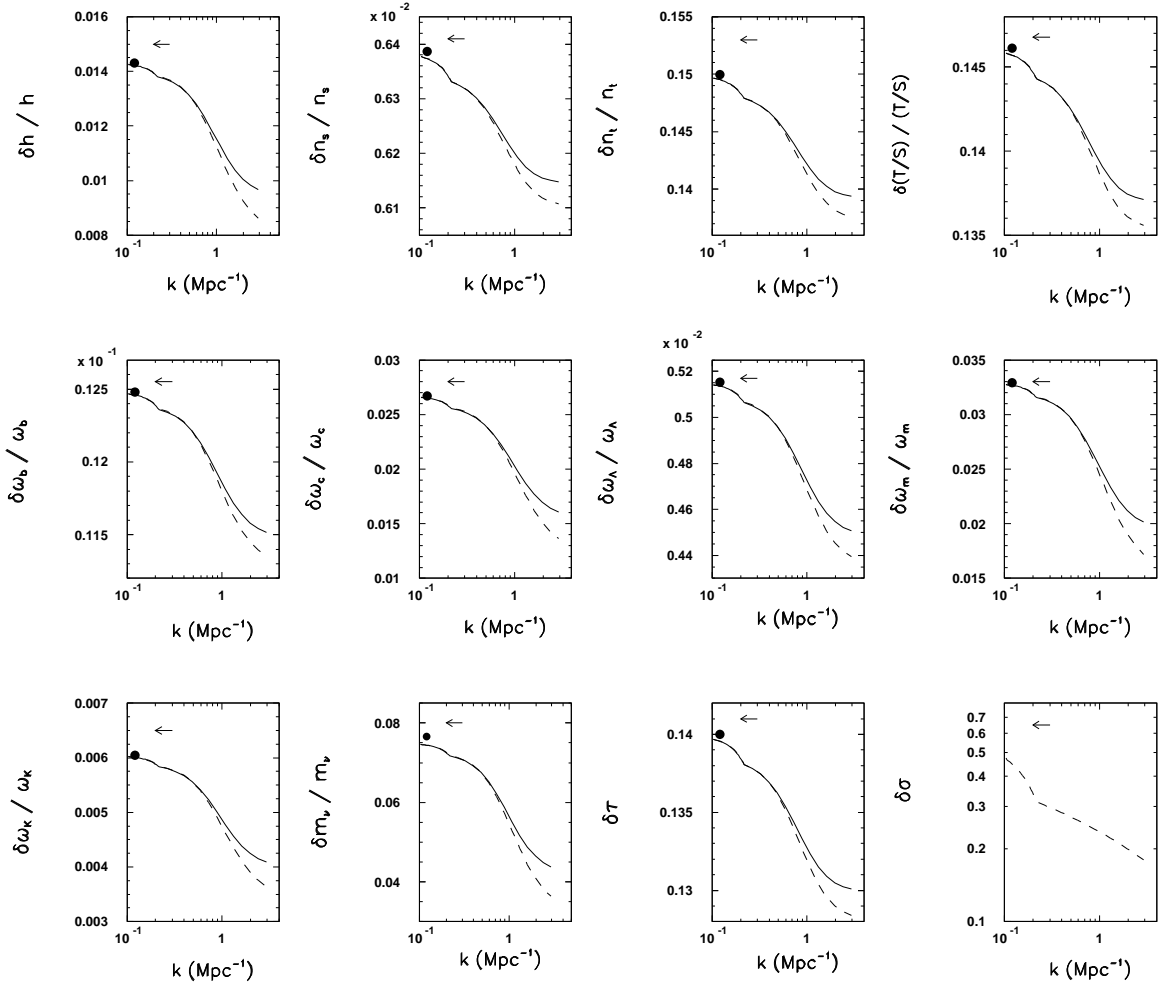


Fig. 8.—  $1 - \sigma$  errors on the estimates of the cosmological parameters from the combined data sets of PLANCK and SDSS when: the linear matter power spectrum is used (continuous lines), the matter power spectrum is corrected for nonlinear effects and redshift distortions (dashed lines). In each case we indicate by the filled circle the  $1 - \sigma$  error obtained by PLANCK alone from anisotropy and polarization data. The arrow indicates the maximum  $k$  accessible to the SDSS.

Figure 8 presents the  $1 - \sigma$  errors on the estimates of the cosmological parameters that can be obtained by PLANCK alone when the CMB anisotropy and polarization data are taken into account and when the combined data sets (CMB anisotropy and polarization and matter density fluctuations) are taken into account for different values of  $k_{max}$ . We consider for the PLANCK surveyor a sky coverage  $f_{sky} = 0.85$ . Figure 8 shows that, although the CMB anisotropy and polarization measurements tend to dominate the constraints on most of the cosmological parameters, the additional small scale LSS data ( $k > 0.1 \text{ Mpc}^{-1}$ ) help to break the parameter degeneracies.

## 6. Conclusions

In this paper we study the complementarity between the cosmological information obtainable with the PLANCK surveyor and the large scale structure redshift surveys in  $\Lambda$ CHDM cosmologies.

We compute the initial full phase-space neutrino distribution function for CHDM and  $\Lambda$ CHDM models by using numerical simulations. We start from the HDM density fluctuation power spectrum in the normalization indicated by the analysis of the local cluster X-ray temperature function and derive the initial neutrino phase-space distribution at each spatial wave number  $k$  by using Zel'dovich approximation. The neutrino phase-space distributions obtained in this way are implemented in the CMBFAST code as initial neutrino momentum distributions for the integration of the coupled linearized Einstein, Boltzmann and fluid equations in  $k$ -space and the computation of CMB power spectra and matter transfer functions.

We find that the relative bias between the CMB anisotropy power spectrum and the matter density fluctuations power spectrum in the COBE/DMR normalization is given by

the CDM component normalized to the abundancy of the rich clusters at the present time.

Taking into account the redshift distortions and nonlinear evolutionary effects on the matter density fluctuations power spectrum, we constrain an 11-dimensional parametrization of the  $\Lambda$ CHDM model, when the combined CMB and LSS data are taken into account in the PLANCK and BRG sample of SDSS experimental specifications. We find that, depending on the maximum spatial wave number, the combined CMB and LSS data can better constrain most of the cosmological parameters.

It is a pleasure to thank U. Seljak and M. Zaldarriaga for the use of the CMBFAST code (v3.2) employed in the computation of the CMB power spectra and of the matter transfer functions.

## REFERENCES

- Ambrosio, M., Atolini, R., Arano, C., et al. (MACRO Collab.), 1998, Phys. Lett. B, 434, 451
- Balbi, A., Ade, P., Bock, J., et al., 2000, preprint astro-ph/0005124
- Bardeen, J.M., Bond, J.R., Kaiser, N., Szalay, A.S., 1986, ApJ, 304, 15
- Bennett, C.L., Banday, A.J., Górski, K.M., et al. 1996, ApJ, 464, L1
- Bertschinger, E., Górski, K.M., Dekel, A., 1990, Nature, 345, 507
- Bertschinger, E., Dekel, A., Faber, S.M., Dressler, A., Burstein, D., 1990, ApJ, 364, 370
- Bertschinger, E., 1995, [http : //arcturus.mit.edu/cosmics](http://arcturus.mit.edu/cosmics)
- Bond, J.R., Szalay, A.S., ApJ, 1983, 274, 443
- Bond, J.R., Jaffe, A.H., Knox, L., 1998, Phys. Rev. D, 2117, 1998
- Bunn, E.F., White, M., 1997, ApJ. 480, 6
- Dekel, A., 1994, ARA&A, 32, 371
- Dodelson, S., Gates, E., Turner, M.S., 1996, Science, 274, 69
- Efstathiou, G., Eastwood, J.W., 1981, MNRAS, 194, 503
- Efstathiou, G., Bridle, S.L., Lasenby, A.N., et al. 1999, MNRAS, 303, L47-52
- Eisenstein, D.J., Hu, W., Tegmark, M., 1998, ApJ, 504, L57
- Eisenstein, D.J., Hu, W., 1999a, ApJ, 511, 5
- Eisenstein, D.J., Hu, W., Tegmark, M., 1999b, ApJ, 518, 2

- Eke, V.R., Cole, S., Frenk, C.S., 1996, MNRAS, 282, 263
- Feldman, H.A., Kaiser, N., Peacock, J.A., 1994, ApJ, 426, 23
- Fukuda, Y., Hayakawa, T., Ichihara, E., et al. (Super-Kamiokande Collab.), 1998, Phys. Rev. Lett., 81,1562
- Fukugita, M., Liu, G.C., Sugiyama, N., 1999, Phys. Rev. Lett. 84, 1082
- Ganon, G., Hoffman, Y., 1993, ApJ, 415, L5
- Gawiser, E., 2000, preprint astro-ph/0005475
- Górski, K.M., Hinshaw, G., Banday, A.J., et al. 1994, ApJ 430,L89
- Guth, A., Pi, S.Y., 1981, Phys. Rev. Lett., 49, 1110
- Hamilton, A.J.S., Tegmark, M., 2000, astro-ph/0008392
- Hamilton, A.J.S., Kumar, P., Lu, E., Matthews, A., 1991,ApJ, 374, L1
- Hancock, S., Rocha, G., Lasenby, A.N., et al. 1998, MNRAS, 294, L1
- Hoffman, Y., Ribak, R., 1991, ApJ, 380, L5
- Hockney, R.W., Eastwood, J.W.,1981, Computer Simulations using Particles(New York:McGraw-Hill)
- Hu, W., Eisenstein, D.J., 1998, ApJ, 498, 497
- Jenkins, A., Frenk, C.S., Pearce, F.R., et al., 1998, ApJ, 499, 20
- Juszkiewicz, R., Górski, K., Silk, J., 1987, ApJ, 323, L1
- Jain, B., Mo, H.J., White, S.D.M., 1995, MNRAS, 276, L25

- Lahav, O., Lilje, P.B., Primack, J.R., Ress, M., 1991, MNRAS, 251, 136
- Lange, A.E., Ade, P.A.R., Bock, J.J., et al., 2000, astro-ph/0005004
- Lineweaver, C.H., 1998, astro-ph/9805326
- Ma, C.P., Bertschinger, E., 1994, ApJ, 455, 7
- Ma, C.P., Bertschinger, E., 1995, ApJ, 455, 7
- Ma, C.P., ApJ, 1996, 471, 13
- Ma, C.P., 1998, ApJ, 508, L5
- Ma, C.P., 1997, astro-ph/9904001
- Mo, H.J., Jing, Y.P., Börner, G., 1996
- Peacock, J.A., Dodds, S.J., 1994, MNRAS, 267, 1020
- Peacock, J.A., Dodds, S.J., 1996, MNRAS, 280, L19
- Peacock, J.A., 2000, astro-ph/0002013
- Peebles, P.J.E., 1980, The Large-Scale Structure of the Universe, Princeton Univ. Press,  
Princeton, NJ
- Pen, U.L., 1997, astro-ph/9610147
- Perlmutter S., Aldering G., Deustua S., et al. 1997, Bull. Am. Astron. Soc., 29, 1351
- Popa, L.A., Stefanescu, P., Fabbri, R. 1999, New Astronomy 4, 59
- Popa, L.A., Burigana, C., Finelli, F., Mandolesi, N., 2000, A&A, in press, astro-ph/0009417
- Primack, R.J., Holtzman, J., Klypin, A., Caldwell, D.O., 1995, Phys. Rev. Lett., 74, 12

- Riess, A.G., Filippenko, A.V, Challis, P., et al. 1998, AJ, 116, 1009
- Scott, D., White, M., 1994, in the Proceedings of the CWRU CMB Workshop “2 Years after COBE”, eds. L. Krauss, P. Kerman
- Scott, D., Silk, J., White, M., 1995, Science, 268, 829
- Seljak, U., Zaldarriaga, M., 1996, ApJ 469, 437
- Smoot, G.F., Bennett, C.L., Kogut, A., et al., 1992, ApJ. 396, L1
- Tegmark, M., 1997, Phys. Rev. Lett., 79, 3806
- Tegmark, M., Zaldarriaga, M., 2000, astro-ph/0002091 v2
- Tegmark, M., 1998, ApJ, 502, 1
- Viana, P.T.P., Liddle, A.R., 1996, MNRAS, 281, 323
- Zaldarriaga, M., Seljak, U., 1997, Phys. Rev. D, 55, 1830
- Zaroubi, S., Sugiyama, N., Silk, J., Hoffman, Y., Dekel, A., 1996, astro-ph/9610132
- Zaldarriaga, M. 1997, Phys. Rev. D, 44, 1822
- Zaldarriaga, M., Seljak, U. 1997, Phys. Rev. D, 55, 1830
- Zaldarriaga, M., Spergel, D.N., Seljak, U., ApJ, 488, 1
- Zel’dovich, Ya.B., 1970, A&A, 5, 84
- Wang, Y., Spergel, D.N., Strauss, M.A., 1998, astro-ph/9802231
- Webster, M., Hobson, P.M., Lasenby, A.N., et al., 1998, astro-ph/9802109
- White, M., Gelmini, G., Silk, J., 1995, Phys. Rev. D, 51, 2669

White, S.D.M., Efstathiou, G., Frenk, C.S., 1993, MNRAS, 262, 1023

Wright, E.L., Smoot, G.F., Kogut, A., et al., 1994, ApJ. 420, 1